ELSEVIER

Thermochimica Acta 312 (1998) 47–61

thermochimica acta

Effect of catalyst deactivation on the acid properties of zeolites used for isobutane/butene alkylation

Freddy A. Diaz-Mendoza[1], Leda Pernett-Bolaño[2], Nelson Cardona-Martínez[*]

Department of Chemical Engineering, University of Puerto Rico – Mayagüez Campus, Mayagüez, Puerto Rico 00681-9046

Abstract

Coke formation during the isobutane/butene alkylation reaction over zeolites decreases the acidity and acid strength of the catalysts. Microcalorimetric measurements of the differential heat of pyridine adsorption and FTIR spectroscopy of adsorbed pyridine were used to probe the changes in the acid properties caused by the deactivation processes. Specifically, fresh and deactivated commercial acid catalysts such as REY, USY, and Beta zeolite were studied. The adsorption microcalorimetry and FTIR spectroscopy results demonstrated that USY has the strongest acid sites (both Brønsted and Lewis) and the highest concentration of strong sites followed by REY and then by Beta zeolite. This order is the opposite of that observed for the alkylation catalytic performance of these zeolites. In particular, it seems that having a high concentration of strong Lewis sites promotes catalyst deactivation. The deposits formed during deactivation have a strong paraffinic character, but evidence of olefinic species is also observed. The degree of unsaturation of the surface species formed increases from Beta to USY zeolite, implying that the presence of a high concentration of strong Lewis-acid sites promotes the formation of unsaturated compounds. Brønsted sites with intermediate acid strength appear to be the appropriate sites for maintaining good alkylation catalytic performance. The best catalytic performance and the slowest deactivation were achieved with Beta zeolite, followed by REY and USY with low sodium content. Only butene isomerization was observed for USY with high sodium content. For the active catalysts, the alkylation global reaction route dominates initially, but the amount of alkylation products decreases as the catalyst starts deactivating when oligomerization predominates; and, finally, the catalyst loses most of its activity and isomerization is the only reaction observed. The product distribution obtained suggests that, instead of authentic alkylation, the initial prevalent mechanism is polymerization followed by β-scission. Two deactivation models are proposed to explain the deactivation. The direct obstruction of the alkylation active sites by irreversible adsorption of coke or coke precursors and the indirect obstruction of the active sites by pore blocking or pore filling. © 1998 Elsevier Science B.V.

Keywords: Catalyst deactivation; Zeolites; Isobutane/butene alkylation

1. Introduction

The amendments of the Clean Air Act of 1990 [1] with a view to reducing the volatility and toxicity of gasoline by changing its overall composition have created a renewed interest in developing improved solid catalysts for isoparaffins alkylation (e.g. see Refs. [2,3]). Gasoline reformulation involves a government-mandated aromatics and endpoints reduction that entails a decrease in octane number and, therefore, the quality of the fuel (e.g. Refs. [3,4]). One of the alternatives to boost the octane number of reformulated gasoline is to increase the alkylation capacity of the refining operations. The alkylates produced by the

*Corresponding author.

[1]Universidad del Atlántico Departmento de Ingeniería Química Via, Puerto Colombia Km. 7, Apartado Aéreo 1890, Barranquilla, Colombia.

[2]Same as in Footnote 1.

PII S0040-6031(97)00439-5

reaction of isoparaffins and olefins have remarkable properties for use as reformulated gasoline blending components, such as high octane, low vapor pressure, and low emissions.

The conventional alkylation processing technology uses concentrated sulfuric acid or anhydrous hydrogen fluoride as catalysts (e.g. see Refs. [2,5,6]). There is a high incentive for replacing these processes by new technology that is environmentally more acceptable and safer, such as one based on a solid catalyst [7,8].

The potential of using zeolite catalysts for isobutane/alkene alkylation has been explored over the last three decades by several research groups [5,9–29]. The zeolites used in these studies included X and Y faujasites, ZSM-5, mordenite, Beta, and MCM-22. HY zeolite was found to be active for isobutane/butene alkylation, but NaX, NaY, and ZSM-5 were inactive, and this behavior was attributed to low acidity in the case of NaX, NaY [16], and to the narrow pores in ZSM-5 [24]. When fresh faujasite were exchanged with rare-earth cations, such as Ce^{3+} or La^{3+}, the catalytic performance for isobutane/alkene alkylation was improved (e.g. see Ref. [19]). More recently, it has been found that Beta zeolite has better catalytic performance for isobutane alkylation than USY, mordenite, ZSM-5, and MCM-22 zeolites [27,30].

Under adequate reaction conditions, good activity and product distribution analogous to those found for the liquid catalysts were obtained for all catalysts. After a certain time-on-stream, however, the zeolites deactivate due to the formation of low temperature coke [2]. The yields of alkylate obtained were also too low for an industrial application. The effect of catalyst deactivation on the acid properties of zeolites used for isobutane/butene alkylation is still not completely understood. Also, there are still some unanswered questions regarding the deactivation mechanism for this reaction on zeolites. In this paper, we attempt to provide some insight that should help in the understanding of these processes.

The experimental program used in this study was designed to evaluate the relationship between the changes in the catalytic properties and the changes in the acid properties of commercial acid catalysts such as REY, USY, and Beta zeolite when they lose their activity after isobutane/1-butene alkylation. Microcalorimetric measurements of the heat of adsorption of pyridine at 473 K were used to determine both the acid-site numbers and strengths for fresh and deactivated zeolites. IR spectroscopy was employed to determine the types of acid sites present on these samples and to determine the nature of the adsorbed species formed during deactivation.

We observe that the formation of low-temperature coke during the isobutane/butene alkylation reaction causes a significant decrease in the acidity and acid strength of the catalysts. Among the zeolites studied, USY has the strongest acid sites (both Brønsted and Lewis) and the highest concentration of strong sites followed by REY, and then by Beta zeolite. This order is the opposite of that observed for the alkylation catalytic performance of these zeolites. Having a high concentration of strong Lewis sites seems to promote catalyst deactivation. The FTIR spectroscopy results demonstrated that the deposits formed during deactivation have a strong paraffinic character, but evidence for olefinic species was also observed.

The degree of unsaturation of the surface species formed increased from Beta to USY zeolite, implying that the presence of a high concentration of strong Lewis-acid sites promotes the formation of unsaturated compounds. Brønsted sites with intermediate acid strength appear to be the appropriate sites for maintaining good alkylation catalytic performance. The combination of results from the different techniques provided evidence that two deactivation mechanisms might be occurring under our reaction conditions.

2. Experimental

2.1. The catalysts

The catalysts studied were samples of commercial zeolites provided by Grace – Davison Division – and were used without further modifications. The physical properties of these catalysts are summarized in Table 1. The low sodium ultrastable faujasite (USY) zeolite was prepared by subjecting the parent NaUSY catalyst to ion exchanges with ammonium nitrate and calcinations to reduce the sodium content. The rare-earth exchanged faujasite (REY) zeolite was also prepared from NaUSY by ion exchange. Ammonium nitrate was used first to decrease the sodium content, and then the rare-earth nitrates were used to add the appropriate cations.

Table 1
Properties of catalysts

Sample	NaUSY	USY	REY	Beta
Supplier	Grace	Grace	Grace	Grace
SiO_2/Al_2O_3	5.41	5.48	5.42	29.96
RE_2O_3 (wt%)			12.21 [a]	
Na_2O (wt%)	4.09	0.69	0.94	0.13
Crystallinity (%)	83	92	48	120
Surface area (m^2/g)	697	768	770	664
Unit cell (Å)	24.55	24.59	24.71	NA [b]

[a] The rare-earth oxide composition was 23.8% LaO_3, 48.8% CeO_2, 5.9% Pr_6O_{11}, 20.4% Nd_2O_3, 1.0% Sm_2O_3, and 0.1% Yb_2O_3.
[b] Information not available.

2.2. Alkylation experiments

A high-pressure fixed-bed reactor was used to study the activity and selectivity of the zeolites during the alkylation reaction as a function of time-on-stream and to obtain the deactivated zeolite samples. The apparatus used is similar to that employed by Weitkamp [19]. A schematic representation of the reaction system is shown in Fig. 1. The main components of the reaction apparatus are: a pressure vessel equipped with a magnetically driven stirrer for preparation and storage of the reactive mixture, an ISCO syringe pump to feed the reactants without pulsations and with a constant flow, a Tescom back-pressure regulator to control the reactor pressure, and a stainless-steel fixed-bed reactor. The reactor used is 15 cm long and has a 9.5 mm diameter.

Before each experiment, the reactor was cleaned with acetone and dried in a furnace at 413 K, then the complete flow system was purged overnight with 80 cm^3/min of dry nitrogen at room temperature. The top of the reactor was filled with an inert material (Ottawa sand from U. S. Silica, particle size 0.25–0.50 mm) to serve as a preheating zone while the catalyst was supported in the lower third of the reactor with glass wool. Each catalyst was pressed binder-free at 69 MPa, ground to particle sizes between 0.25 and 0.50 mm, and dried at 413 K for 2 h prior to being weighed and loaded into the reactor. About 1 g of sample was used in each experiment.

The reactor temperature was controlled using a furnace and a temperature controller. A 1/16-inch

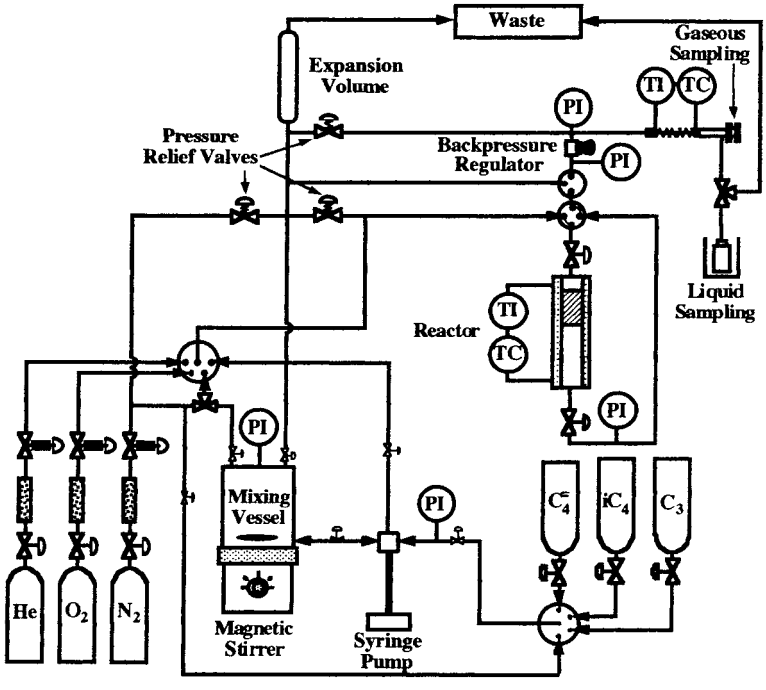

Fig. 1. Schematic of the reaction system.

thermocouple located inside the bed was used to measure the reaction temperature. The reaction temperature and pressure used were 353 K and 400 psi (2.7 MPa), respectively, and the volumetric feed flow rate at room temperature was 10 cm^3/h. These conditions corresponded to weight hourly velocities between 4 and 4.6 h^{-1}.

Isobutane-to-1-butene molar ratios between 10 and 11.3 were used for all experiments in an attempt to suppress undesirable side reactions of the olefins [20–22]. Both, the isobutane (Air Products) and the 1-butene (Matheson) were better than 99% pure and were used without further purification. Propane (Air Products, better than 99% purity) served as an internal standard for GC analyses. Propane does not react at the experimental conditions used [19]. Samples of the reactive mixture were analyzed with a GC to confirm that the desired ratios were present in the mixing vessel.

The catalysts were activated in flowing dry nitrogen (90 cm^3/min) at 623 K for 2 h and then cooled to the reaction temperature of 353 K while maintaining the nitrogen flow. This was followed by isolating the reactor in ca. 2.72 MPa of nitrogen. When the flow of the reactive mixture at the desired pressure was established, a four-port valve was switched to start feeding the reactants into the reactor. The first product sample was collected when the first drop of liquid was observed at the reactor outlet. A short transparent Teflon line at the reactor outlet was used to visually detect the liquid product. Subsequent samples were gathered at time intervals of 2–5 min, initially, and farther apart as the time-on-stream increased. The reaction was continued until the catalyst deactivated as ascertained by the product analyses. After the reaction was completed, the reactor was purged with nitrogen for 20 min at the reaction temperature and the deactivated sample stored in nitrogen in a desiccator for subsequent analysis.

A Shimadzu 9A gas chromatogragh, with a flame ionization detector and a 60 m capillary column (J & W DB-1), was used for analysis of the hydrocarbon products and the reactive mixture. Gaseous samples of the products were collected from a chamber at the reactor outlet kept at 473 K into sampling cylinders and stored for subsequent analysis. This procedure allowed the collection of multiple samples at frequent intervals while the initial samples were analyzed. When ready for analysis, the cylinders were heated again to 473 K and a gaseous sample withdrawn and injected into the GC. After each use, the cylinders were cleaned with acetone, dried at 413 K, and evacuated with an oil-free vacuum pump. The used cylinders were randomly analyzed to confirm that there was no cross contamination between runs. Integral liquid samples were collected into a stainless-steel cylinder kept at 203 K and stored for later analysis. These samples were useful for qualitative assignment of GC peaks.

Assignments of the reactants and products chromatographic peaks up to C_9 were based on commercially available reference standards (Supelco alkylate standard and olefin standard) and retention-index data compiled in the literature [31]. No attempt was made to identify C_{10} or higher hydrocarbons. Two supplementary procedures were used to identify octenes with retention times close to those for octanes. Some selected samples were analyzed using a Hewlett–Packard 5790 gas chromatograph equipped with a Hewlett–Packard 5970A mass spectrometer. In the second procedure, an additional analysis method for the liquid samples was developed using the GC/FID with an absorber precolumn. The details of this method are given in Ref. [32].

2.3. Adsorption microcalorimetry experiments

The microcalorimetry apparatus used is similar to that described in Ref. [33]. It consists of a Setaram C80D heat-flow microcalorimeter of the Calvet type with a sensitivity of 0.1 mW, connected to a stainless-steel, calibrated, volumetric system. The calorimeter is placed on a heavy-duty jack that permits the calorimeter to be moved during pretreatment of the sample under study without sample exposure to air.

Pressures are measured by means of either a MKS Baratron Model 615 AD capacitance manometer for pressures between 1×10^{-5} and 10 torr (1 torr=133.3 Pa) or an MKS Baratron Model 590 HA capacitance manometer for pressures between 1×10^{-3} and 1000 torr.

The entire calorimetric system is thermally insulated. The temperature of the volumetric system is kept constant at 345 K using a PID controller. The temperatures of the cells and dosing volume are measured using a pair of precision platinum resistance

temperature devices (RTD). The dosing volume is attached to a diffusion-pumped glass vacuum system with an ultimate dynamic pressure of 4×10^{-7} torr and to a gas-handling and purification system.

For the fresh catalysts, between 150 and 350 mg of zeolite were placed in the sample cell, and the cells were slowly evacuated while heating to 623 K. Following this initial evacuation, the catalyst was pretreated at 623 K for 2 h in ca. 700 torr of static helium. During this treatment, helium was periodically added and evacuated from the cells. This procedure was intended to simulate the activation treatment used for the alkylation experiments. The helium was purified by passage through a molecular sieve (3A) trap at 77 K. After sample activation, the sample was cooled, under dynamic vacuum, to room temperature. The calorimeter was lifted by the jack to enclose the cells, and the sample was evacuated overnight to allow the system to reach thermal equilibrium at 473 K. Helium or argon was subsequently used to determine the cells dead volume.

The procedure for the deactivated catalysts was different because we did not want to remove the coke from the surface or modify it significantly. Therefore, the samples were exposed to helium using the same procedure described above, except that the temperature used was 473 K and the treatment performed inside the calorimeter. From 300–500 mg of sample were used for these experiments.

The pyridine (E.M. Science, 99.2% purity) used in these studies was dried by storage over activated molecular sieve (3A) and purified with the freeze–pump–thaw technique before each run. The basic molecule was kept in a constant-temperature bath to produce a vapor pressure of ca. 4.8 torr. A known amount of the base (1–4 μmol) was then placed in the calibrated dosing volume. The probe molecule was subsequently dosed into the calorimeter cells, one cell containing the sample, the other empty cell serving as a reference. The heat released on dosing the base was detected by the calorimeter. The signal from the calorimeter was sent to a strip-chart recorder and to a National Instruments LC ana log-to-digital interface. The signal from the calorimeter amplifier, as well as the pressure and dosing volume temperature, were fed to an Apple Macintosh LCII computer which was programmed to integrate the area under the thermogram, calculate the amount of pyridine adsorbed during the dose (Δn), calculate the integral heat of adsorption (Q), and determine the differential heat of adsorption per mole of adsorbed pyridine as $\Delta Q/\Delta n$. The processing of these data provides a complete characterization of the adsorption process. Integral heat and volumetric isotherms give the total heat and total adsorption, respectively, as a function of pressure. Integral heats, Q, as a function of coverage, provide the overall acid strength of the system. Differential heats of adsorption as a function of coverage provide a description of the acid-strength distribution over the surface of the catalyst. When equilibrium conditions were attained after a dose, that is, constant pressure and no deviation from the calorimetric base line, the cells were isolated and the dosing volume was evacuated to decrease the amount of air admitted to the system through small leaks. The above procedure was followed repeatedly. Data were collected until the differential heat of adsorption was in the region of H-bonding on silica [33]. A typical adsorption isotherm was built sequentially from ≈60 to 80 consecutive doses within 6 and 10 days.

2.4. Ftir spectroscopy experiments

Infrared spectroscopy of adsorbed pyridine was used to determine the types of acid sites present on the samples and to study the changes in acidity caused by surface species formed during deactivation. The spectral region from 1400 to 1650 cm^{-1} is particularly important for acidity characterization since this range contains IR absorption frequencies expected for coordinated pyridine, pyridinium ion and H-bonded pyridine. The apparatus and procedure used are described below.

All infrared spectra were taken at room temperature with a Nicolet Magna 550 FTIR spectrometer. A conventional flow system was used to treat the samples and to adsorb pyridine. The details of the flow system are given in Ref. [32]. The Pyrex cell used to collect all spectra has a 25 mm diameter, is 150 mm long, and has 32 mm CaF_2 windows connected with ultratorr fittings (PR valve and fittings).

In a typical experiment, ca. 40 mg of sample was pressed into a self-supported 1 cm wafer. The disk was placed in the sample holder and then pretreated in

flowing helium (80 cm^3/min) for 2 h. The fresh catalysts were activated at 623 K while the deactivated zeolites were treated up to 473 K. After the activation, the sample was cooled to room temperature and an initial spectrum collected. This spectrum was subtracted from the subsequent pyridne spectra with baseline correction to show only the pyridine bands. The deactivated catalysts were purged at room temperature for 1 h followed by collecting a spectrum to check the state of the surface. These samples were subsequently heated in flowing helium for 1 h each to 323, 373, 423, and 473 K. After each treatment, a spectrum was collected at room temperature to check if the treatment modified the surface species. Pyridine was adsorbed on the catalysts by passing a pyridine saturated helium stream through the cell at 473 K for 1 h. The pyridine saturator was kept at 273 K. Both pyridine and helium were purified as described above. After the adsorption period, the gas-phase pyridine and any weakly adsorbed pyridine were removed from the cell by flowing helium (100 cm^3/min) for 2 h at 473 K, before cooling to room temperature and collecting a spectrum. Pyridine was subsequently desorbed in flowing helium at 623 and 723 K for 1 h and additional room-temperature spectra collected.

The procedure for the identification of the acid types present is straightforward and has been described for samples equilibrated with a high pyridine pressure and, subsequently, evacuated at increasing temperatures [33–36]. H-bonded pyridine (HPY) on the surface can be detected by a strong 19*b* absorption at 1445 cm^{-1} coupled with an 8*a* band having a weaker peak at 1595 cm^{-1}. Both the 19*a* and 8*b* bands can be observed, but they are much weaker. If Lewis-acid sites are present, a 19*b* band will appear at 1450 cm^{-1} and a distinct 8*a* band will appear at a frequency higher than 1600 cm^{-1}. If Brønsted-acid sites are present on the surface, a weak 19*b* band will appear at 1540 cm^{-1}. This will be present in conjunction with an 8*a* band at 1640 cm^{-}. In addition, the 19*b* band at 1490 cm^{-1}, which overlaps for both Lewis and Brønsted sites, is much stronger when Brønsted sites are present relative to the Lewis-acid peak at 1450 cm^{-1}. The 8*a* and 19*a* bands correspond to symmetric ring vibrations, while the 8*b* and 19*b* bands correspond to antisymmetric ring vibrations.

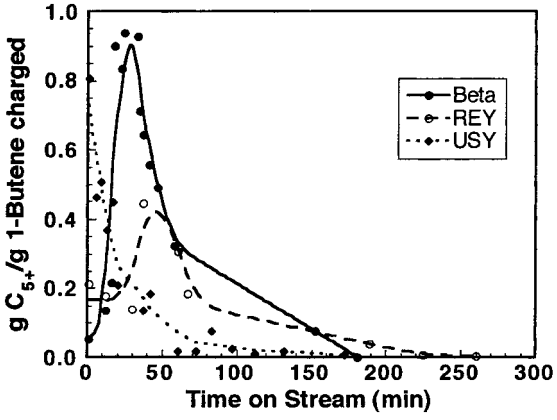

Fig. 2. Effect of time-on-stream on the alkylate yield for the different zeolites; (——●——) Beta; (–⊖–) REY; and (- -◆- -) USY.

3. Results and discussion

3.1. Alkylation results

During the initial stage of the reaction, all catalysts are selective and no olefinic or aromatic hydrocarbons are detected in the product stream, only branched paraffins are observed. Fig. 2 shows the alkylate yield as a function of time-on-stream for the different zeolites. The alkylate yield is defined as the ratio of the amount of paraffinic hydrocarbons with five or more carbon atoms (C_{5+}) produced to the amount of 1-butene fed to the reactor. The alkylate yields for Beta and REY pass through maximums of 0.95 and 0.45 g/g butene charged, respectively, before starting to quickly decrease. Note that the small fluctuations in the data presented in this and other figures are caused by experimental errors especially when ratios are calculated. For USY, the initial yield is ca. 0.8 g/g butene charged and its alkylation activity drops faster than for the other zeolites. Probably, our experimental procedure did not have sufficient resolution to notice the maximum in yield for this catalyst. For an idealized alkylation mechanism, the maximum alkylate yield possible is slightly >2 g/g butene charged. Strong olefin adsorption and the accumulation of coke are considered important factors that limit the yield of alkylate [19].

As seen in Fig. 3, initially all catalysts are highly selective toward the alkylate products with values

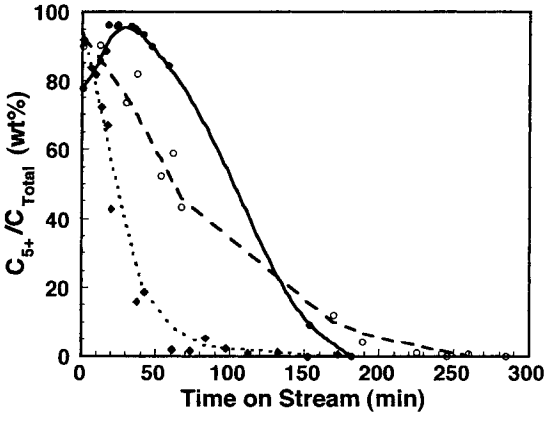

Fig. 3. Effect of time-on-stream on the alkylate selectivity for the different zeolites: (——●——) Beta; (–⊖–) REY; and (- -◆- -) USY).

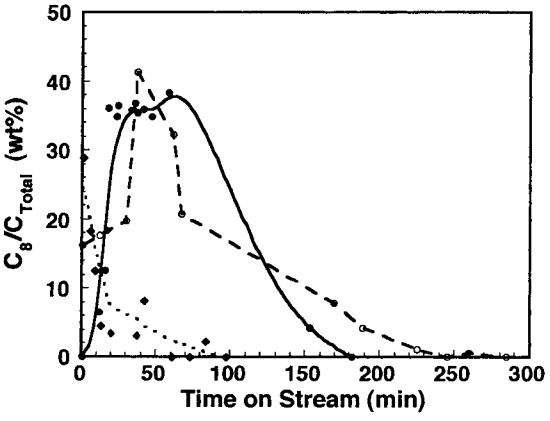

Fig. 4. Effect of time-on-stream on the C_8 selectivity for the different zeolites: (——●——) Beta; (–⊖–) REY; and (- -◆- -) USY.

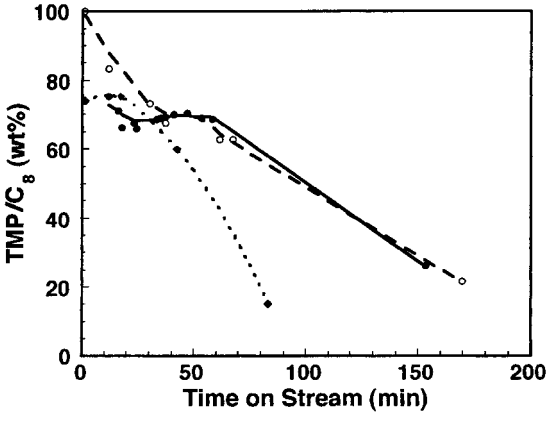

Fig. 5. Effect of time-on-stream on the fraction of trimethylpentanes in the C_8 for the different zeolites: (——●——) Beta; (–⊖–) REY; and (- -◆- -) USY.

close to 100% selectivity. Beta gives the highest selectivity, up to ca. 150 min, after which REY is slightly more selective. USY gives the lowest selectivity for all times. For low times-on-stream, a significant fraction of the alkylate products corresponds to C_8 hydrocarbons as shown in Fig. 4. Most of these C_8 molecules are trimethylpentanes, as depicted in Fig. 5. In both cases, Beta and REY display the best selectivities. The relatively low concentrations of C_8 isomers in the alkylate product are caused by the formation of molecules between C_5 and C_7, most probably through β-scission of oligomers. From the results presented above, we can conclude that the best catalytic performance and slowest deactivation were achieved with Beta zeolite, followed by REY, and USY with low sodium content. Only butene isomerization was observed for the high sodium content faujasite (NaUSY). The lack of alkylation activity for this zeolite appears to be caused by the high sodium content that significantly reduces its acidity. There are many examples in the literature of the effect of sodium on the acidity of zeolites (e.g. see Refs. [37,38] and references therein). Poisoning with sodium has also been shown to drastically reduce the cracking activity of zeolites (e.g. see Ref. [39]). Our results are also consistent with those of Minachev et al. [16] who found that the sodium forms of X and Y zeolites were not active for isobutane alkylation and that ion exchange with rare earths improved the yield and quality of the product. Corma et al. [27] on the other hand, found that Beta zeolite displayed better catalytic performance for isobutane alkylation than USY, mordenite, ZSM-5, and MCM-22 zeolites.

After a certain time, butenes (1-butene, *cis*, and *ttans* 2-butene) and octenes are detected in the product stream for all active catalysts. Fig. 6 shows the composition of the C_8 fraction (paraffinic vs. olefinic C_8) for the zeolites. It is clearly seen that after ca. 35 min in case of USY, and ca. 60 min in case of Beta and REY, and quality of the products deteriorates rapidly and butene oligomerization products start to dominate the C_8 pool. The amount of olefins in the product

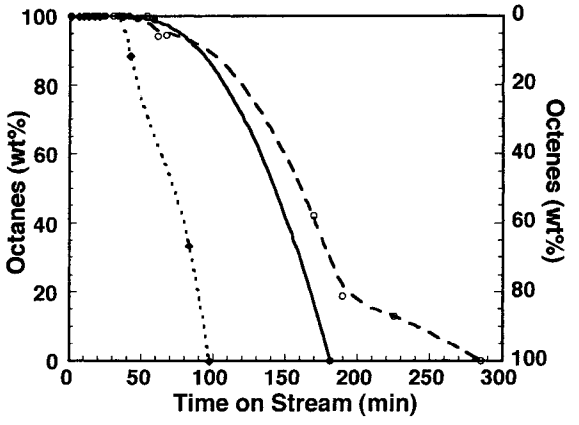

Fig. 6. Effect of time-on-stream on the composition of the C_8 fraction (paraffinic vs. olefinic C_8) for the different zeolites: (——●——) Beta; (–⊖–) REY; and (- -◆- -) USY.

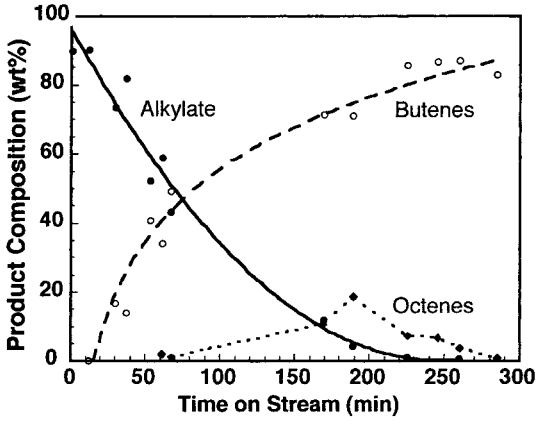

Fig. 7. Effect of time-on-stream on the product composition for REY: (——●——) Alkylate; (–⊖–) butenes; and (- -◆- -) octenes.

stream increases quickly with the reaction time until eventually no alkylation products are detectable. Only butene isomerization and oligomerization products are observed during this stage. Finally, the oligomerization route ceases and only isomerization is perceived. At this point, the catalyst is deactivated by the formation of coke. Two deactivation models may be proposed to explain the deactivation. The first one is a direct obstruction of the alkylation active sites by irreversible adsorption of coke or coke precursors. The second model is an indirect obstruction of the active sites by pore blocking or pore filling.

The premise that both processes might be occurring for the catalysts used is suggested by an analysis of the behavior observed by the product composition as the catalysts deactivate. For example, Fig. 7 shows how the product composition changes with time-on-stream for REY. It is obvious from the figure that, initially, only alkylation products are detected. These are probably formed over strong Brønsted-acid sites [26]. Simultaneously, side reactions might be occurring to form coke precursors that can irreversibly adsorb on the strong sites (deactivation model I). This causes a loss in hydride transfer capacity that is indispensable for alkylation and the alkylation activity starts to drop. As this happens, secondary reaction routes like butene isomerization and oligomerization start to predominate. This is manifested first by the increase in butenes concentration, then by an increase in octenes concentration. The C_8 olefins are produced by desorption of surface species formed from β-scission of oligomers. The olefin oligomerization reaches a maximum before stopping completely. At this point, it is possible that the chain growth of polyolefinic species is sufficient to start blocking or filling the pores that give access to the interior of the zeolite (deactivation model II) or that all the active sites are covered by coke. Finally, the catalyst is only active for butene isomerization that most probably takes place on exterior weak acid sites such as those found for NaUSY. The results for Beta and USY zeolites were equivalent.

According to the mechanism generally proposed for the alkylation of isobutane (e.g. [14,19,23–26,40]), the first steps of the reaction are the olefin protonation on a Brønsted site, followed by abstraction of a hydride ion to give *n*-butane and the *tert*-butyl carbenium ion. If this is true, a higher hydride transfer activity will enhance the formation of *n*-butane and *tert*-butyl carbenium ion, and as a result the formation of alkylate products. This behavior is consistent with our results shown in Fig. 8, where we can see that the order to catalytic activity corresponds to the order of *n*-butane formation. The formation of *n*-butane may then be used as a measure of the zeolite capacity for hydride transfer as has been suggested by Corma et al. [26].

The trimethylpentanes (TMP) are commonly considered to be formed by the reaction of the *tert*-butyl carbenium ion with an olefin, while the dimethylhexanes (DMH) are believed to be formed by the olefin

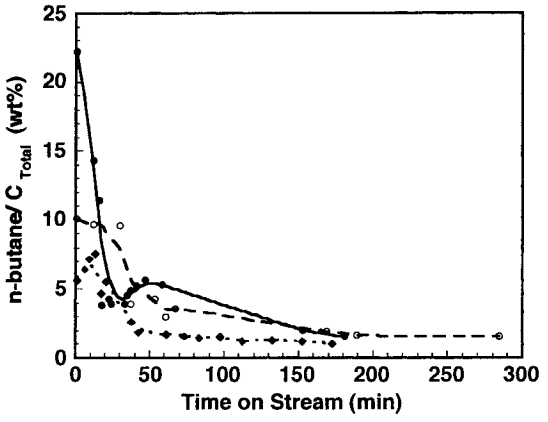

Fig. 8. Effect of time-on-stream on the *n*-butane composition for the different zeolites: (——●——) Beta; (–⊖–) REY; and (- -◆- -) USY.

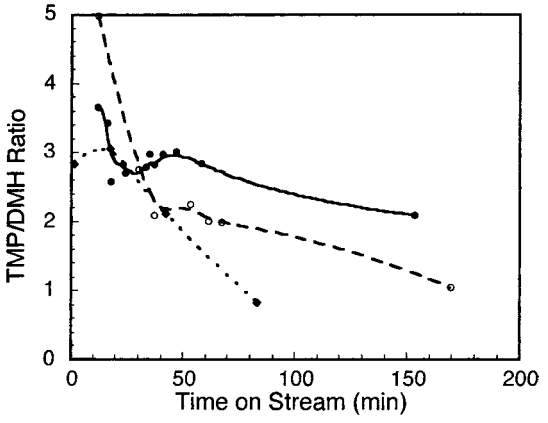

Fig. 9. Effect of time-on-stream on the TMP/DMH ratio for the different zeolites: (——●——) Beta; (–⊖–) REY; and (- -◆- -) USY.

dimerization. A comparison of the TMP/DMH ratio for the zeolites studied (Fig. 9) demonstrates that this ratio decreases as the time of reaction increases. Corma et al. [26] have also recommended the use of this ratio to measure the zeolite capacity for alkylation against oligomerization. From our results it is evident that the sites active for alkylation are the first to deactivate while those responsible for oligomerization persist for a longer time.

Another possible route to form the alkylate product is by polymerization followed by β-scission. The high concentration of hydrocarbon molecules in the C_5–C_7 range (Table 2) indicates that the contribution from this route is important. According to the product distribution observed, it seems that the predominant routes for the formation of the C_5–C_7 molecules, and possibly the C_8 molecules, is β-scission of C_{12}^+ and C_{16}^+ carbenium ions. If this is true, it is likely that the C_8 molecules are formed predominantly through this route rather than from authentic alkylation [24,40]. From the high initial concentration of paraffinic C_5–C_7 hydrocarbons, we would expect that some low molecular weight olefins should be observed in the products, but none were detected. It is possible that these products are not detected because they rapidly readsorb on the surface and continue growing.

Table 2
C_4–C_{9+} product distribution for low times-on-stream (wt%)

Zeolite	USY		REY		Beta	
Time-on-stream, min	1	16	1	10	1	16
1-butene		2.0				
2-butene	2.5	26.2				
n-butene	5.6	4.7	10.1	9.7	22.2	3.8
C_5	36.1	26.8	43.6	41.8	65.0	21.5
C_6	16.9	15.1	21.9	22.8	12.7	15.9
C_7	8.3	6.8	8.2	8.0	3.9	15.9
C_8	29.0	18.4	16.2	17.7		36.2
C_{9+}	1.6					6.6

3.2. Microcalorimetry and FTIR spectroscopy results

The IR spectra of pyridine adsorbed on the fresh zeolites at 473 K, followed by desorption at 623 and 673 K, are shown in Figs. 10–12. The spectra show that all zeolites studied possess both Lewis- and Brønsted-acid sites. The relative concentrations of Brønsted- and Lewis-acid sites may be qualitatively estimated by comparing the intensities of the bands ca. 1545 cm^{-1} to the intensities of the bands ca. 1455 cm^{-1}. The values of this ratio are 1.5 for Beta, 11.7 for REY, and 0.8 for USY. Hence, incorporating rare earths onto the USY zeolite significantly increases the relative concentration of Brønsted-acid sites. Beta also has a higher relative concentration of acid sites than USY. Desorption of pyridine from the catalysts at increasing temperatures provokes a significant decrease in the intensity of all bands. This result implies that all zeolites studied have both,

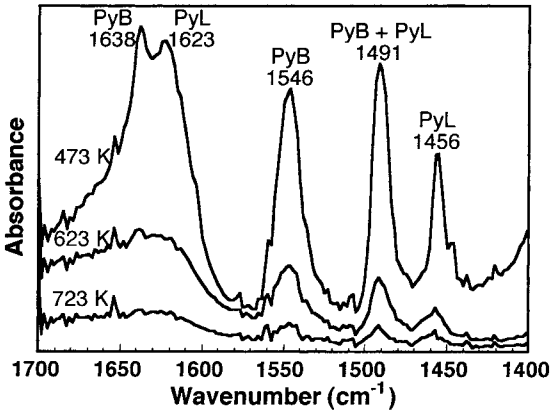

Fig. 10. IR spectra of pyridine adsorbed on fresh Beta zeolite at 473 K followed by desorption in flowing He at the indicated temperatures. LPY – Peak corresponding to pyridine bonded to a Lewis-acid site; and BPY – peak corresponding to pyridine bonded to a Brønsted-acid site.

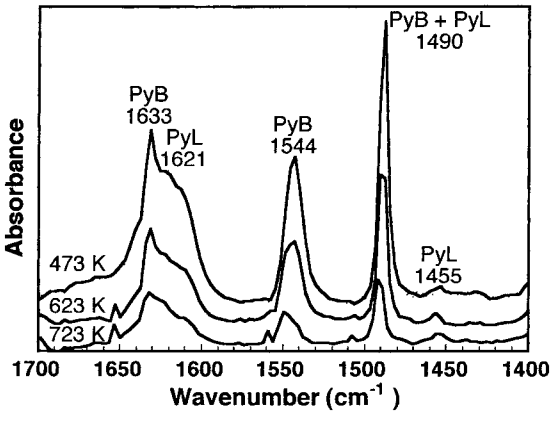

Fig. 11. IR spectra of pyridine adsorbed on fresh REY zeolite at 473 K followed by desorption in flowing He at the indicated temperatures. LPY – Peak corresponding to pyridine bonded to a Lewis-acid site; and BPY – peak corresponding to pyridine bonded to a Brønsted-acid site.

Brønsted- and Lewis-acid sites with a distribution of acid strength.

A comparison of the decrease in the intensity of the band ca. 1545 cm^{-1} with the increase in the desorption temperature should give us a qualitative measure of the Brønsted-acid strength. For USY, the decrease in intensity is ca. 30% at 623 K and 80% at 723 K. In the case of REY, the intensity drops by ca. 45% at 623 K

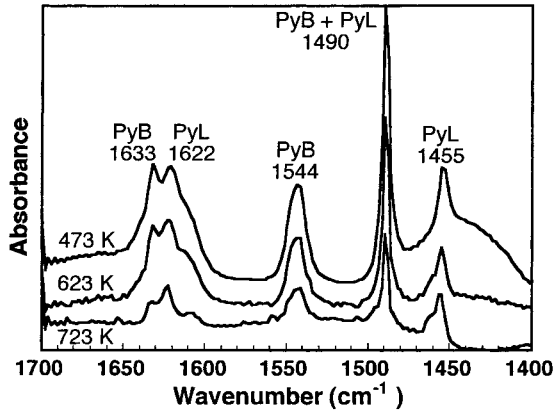

Fig. 12. IR spectra of pyridine adsorbed on fresh USY zeolite at 473 K followed by desorption in flowing He at the indicated temperatures. LPY – Peak corresponding to pyridine bonded to a Lewis-acid sites; and BPY – peak corresponding to pyridine bonded to a Brønsted-acid site.

and 85% at 723 K. Finally, for Beta, the reduction is ca. 73% at 623 K and 91% at 723 K. Consequently, USY has the highest fraction of strong Brønsted sites, followed by REY and, finally, Beta has the smallest fraction. USY also has the highest concentration of strong Lewis-acid sites since ca. 41% of the pyridine remained at 723 K. REY, on the other hand, has few Lewis sites, but most of these are strong as shown by the small reduction in the intensity of the band at 1455 cm^{-1} (only ca. 30% overall). Again, Beta has the smallest fraction of strong Lewis-acid sites (ca. 94% reduction overall).

All of these results are consistent with the adsorption microcalorimetry results depicted in Figs. 13–15 and in Table 3. Note that data for two experiments using fresh USY are shown to illustrate the reproducibility of our method. From the results shown, clearly fresh USY has the strongest sites (initial differential heat of ca. 260 kJ/mol) and the highest concentration of strong sites (ca. 250 μmol/g with heats higher than 200 kJ/mol). The differential heats of pyridine adsorption found for USY are consistent with the range of values reported in the literature [37,38]. The initial differential heats of adsorption for fresh REY and fresh Beta are 230 and 255 kJ/mol, respectively. Both however, have low concentrations of strong sites (ca. 35 μmol/g with heats >200 kJ/mol).

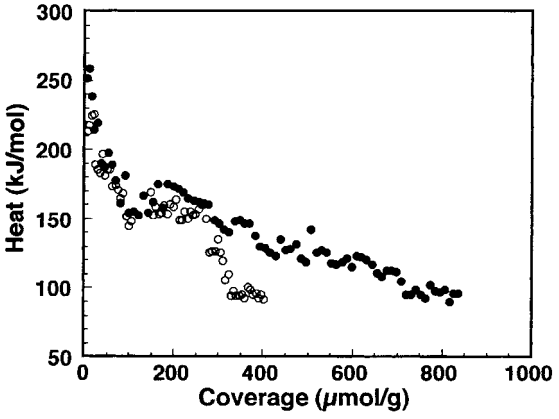

Fig. 13. Differential heat of adsorption for pyridine adsorbed on Beta zeolite at 473 K ((●) fresh; and (○) deactivated).

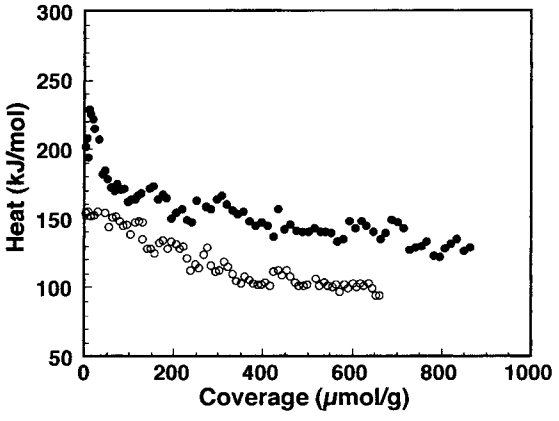

Fig. 14. Differential heat of adsorption for pyridine adsorbed on REY zeolite at 473 K ((●) fresh; and (○) deactivated).

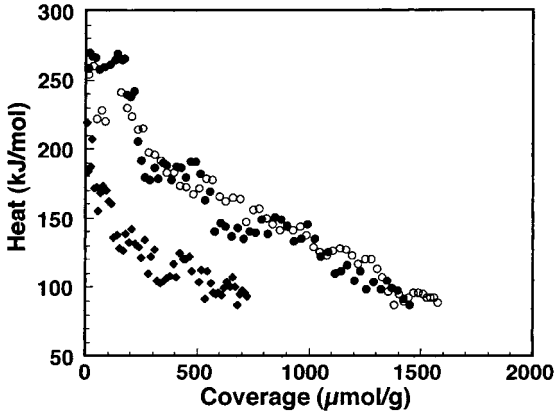

Fig. 15. Differential heat of adsorption for pyridine adsorbed on USY zeolite at 473 K ((●) fresh run 1; (○) fresh run 2; and (◆) deactivated).

To the best of our knowledge this is the first time that Beta zeolite is studied using adsorption microcalorimetry and the first time that REY is studied using pyridine adsorption microcalorimetry. Two additional studies using ammonia adsorption on LaY at 298 K were found [41,42], reporting significantly lower differential heats. It is well known that low adsorption temperatures smooth details in the differential heat vs. coverage curves, and the adsorbent appears to be more energetically homogeneous than it really is [33,38]. In addition, it has been shown [38,43] that ammonia is a weaker base than pyridine in the gas phase. The first effect does not allow the determination of the true acid-strength distribution while the second significantly decreases the measured differential heats, thus these results are unreliable and useless

Table 3
Summary of calorimetry results

Catalyst		Initial heat/ (kJ/mol)	Total acidity [a]/ (μmol/g)	Average integral heat [b]/ (kJ/mol)
Beta	fresh	255	800	140
	deactivated	225	320	169
REY	fresh	230	900 [c]	144
	deactivated	155	600	117
USY	fresh	260	1350	167
	deactivated	215	650	123

[a] Coverage when the differential heat drops to 95 kJ/mol.
[b] Integral heat of pyridine adsorption when the differential heat of adsorption decreases to 95 kJ/mol $\{q_{av} = Q_{95}/n_{95}\}$.
[c] Value was underestimated (see Section 3 for explanation).

for comparison with the values obtained in this work.

We define the total number of acid sites (total acidity) of the zeolites as the amount of pyridine adsorbed with heats >95 kJ/mol. This value corresponds to the differential heat of pyridine adsorbed on SiO_2 at 473 K [33]. The order of total acidity is as follows: USY>REY>Beta (Table 3). For REY, the total acidity should be higher than the value reported in Table 3 because, using the changes observed in the adsorption isotherm, the experiment was stopped before the heats dropped to 95 kJ/mol. Then, the slope of the adsorption isotherm began to decrease which means that we were not far from the desired region of heats. The average integral heat provides a measure of the overall acid strength. This quantity is estimated by dividing the integral heat corresponding to a differential heat of 95 kJ/mol by the total acidity ($q_{av}=Q_{95}/n_{95}$). As shown in Table 3 again, the relative order of overall acid strength is the following: USY>REY>Beta. This order is the opposite of the order observed for the alkylation catalytic performance of these zeolites. This result suggests that the zeolites with the highest acid strength are not the best catalysts for alkylation. In particular, it seems that having a high concentration of strong Lewis sites is detrimental for maintaining good alkylation catalytic performance.

The results for the deactivated samples reveal that the formation of coke causes drastic changes in the acidity of the catalysts. The initial differential heat, the total acidity, and the average integral heat decrease significantly for all zeolites, except the average integral heat for Beta which increases. Hence, for the deactivated samples, pyridine does not have access to a significant fraction of the acid sites originally available on the fresh samples; moreover, most of the sites that are available for pyridine adsorption on the deactivated samples are generally weaker than those present on the fresh zeolites. The exception is Beta that loses a higher fraction of the intermediate strength sites. If the deactivation was mainly produced by irreversible adsorption of coke or coke precursors (deactivation model I), we would expect that most of the strongest sites would be lost and most of the weaker sites to be available for adsorption. The fact that, for all catalysts a fraction of the intermediate strength sites is lost (specially for Beta), and that some strong sites (most probably external sites) are still available for USY and Beta is additional evidence supporting a contribution of pore blocking or pore filling (deactivation model II) to the deactivation of these zeolites.

We are aware of only one additional study, where the effect of deactivation on the acidity of zeolites has been studied using adsorption microcalorimetry [44,45]. In that study, the acid strength distributions of H-mordenite, H-offretite and HZSM-5 were determined before and after their use as catalysts in methanol conversion at 650 K. Agreeing with our work, the acidity of the used catalysts was considerably lower than that of the fresh materials due to coke deposition. However, in this case the strongest acid sites on all surface disappeared or decreased in strength. For the used ZSM-5 catalyst, a decrease in the number of strong acid sites was observed, but no decrease in activity was found. It can be concluded that only a fraction of the acid sites titrated by ammonia was necessary to maintain high catalytic activity and that the different behavior of mordenite and ZSM-5 zeolite during the same catalytic reaction was probably the result of their different pore structures. Again, the strongest sites are not necessarily the active sites.

Figs. 16 and 17 show the infrared spectra of deactivated Beta and USY zeolites after flowing He at 473 K. Bands corresponding to paraffin species are observed for deactivated Beta (Fig. 16) in the region of the CH stretching modes (ν_{as} [CH_3]=2959 cm^{-1};

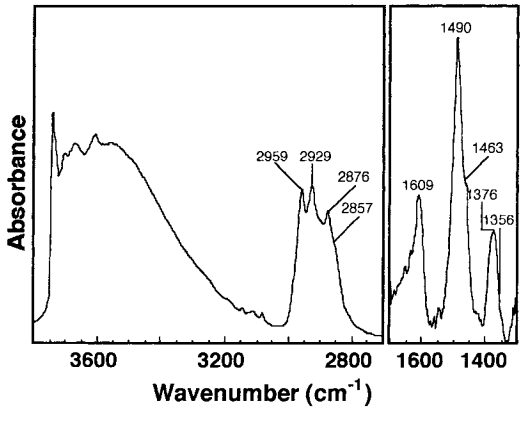

Fig. 16. IR spectrum of deactivated Beta zeolite after flowing He at 473 K.

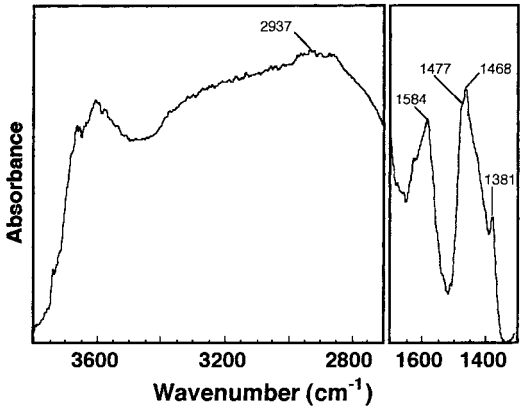

Fig. 17. IR spectrum of deactivated USY zeolite after flowing He at 473 K.

ν_{as} [CH_2]=2929 cm^{-1}; ν_s [CH_3]=2876 cm^{-1}; ν_{as} [CH_2]=2857 cm^{-1}) [46,47]. Also, the region between 1500 and 1300 cm^{-1} exhibited the corresponding CH deformation bands, namely δ_{as}[CH_3=1490 cm^{-1}; δ_{as}[CH_2=1463 cm^{-1} (shoulder); δ_s[CH_3=1376 cm^{-1}; δ_s[CH_2=1351 cm^{-1} (shoulder). These results indicate that the coke on deactivated Beta zeolite has a strong paraffinic character. An additional band is observed at 1609 cm^{-1}. This band is assigned to C=C stretching vibrations of olefinic or polyolefinic species and has been shown to be a suitable measure for the amount of coke deposited [46,47].

The results for deactivated USY are not as obvious as those for deactivated Beta. The bands observed at 1468 and 1381 cm^{-1} might be assigned to CH_2 and CH_3 deformation modes, respectively, but the corresponding bands at 1485–1490 and 1350–1360 cm^{-1} are not present. Also, the region of the CH stretching modes collapsed into one broad band extending from 3450 to 2100 cm^{-1} with a maximum at 2937 cm^{-1}, probably indicating a more complex mixture of surface species. The additional band at 1477 cm^{-1} (shoulder) has been assigned to oligomer formation after 1-butene adsorption at 353 K on LaHY zeolite by Flego et al. [29]. Finally, the position of the coke band ca. 1600 cm^{-1} shifted to 1584 cm^{-1} for deactivated USY. This indicates that the structure of the main components of the coke changed for deactivated USY, most likely in the direction of more unsaturated compounds [46]. These results are consistent with UV–VIS spectra of surface species formed during isobutane alkylation on LaHY zeolite at 353 K that detected both monoenyl and dienyl carbenium ions [29].

We do not observe evidence of the formation of aromatic surface species on any of our samples. This outcome confirms findings using ^{13}C CP/MAS NMR by Stöcker et al. [28], who found that the coke formed on hexagonal or cubic faujasite after isobutane alkylation was not aromatic, and using ^{13}C CP/MAS NMR, UV–VIS, and FTIR by Flego et al. [29], who found similar results for LaHY zeolite.

4. Conclusions

The best catalytic performance for isobutane/1-butene alkylation and slowest deactivation were achieved with Beta zeolite followed by REY and USY with low sodium content. Only butene isomerization was observed for USY with high sodium content. For the active catalysts, the alkylation global reaction route dominates initially, but the amount of alkylation products decreases as the catalyst starts to deactivate when oligomerization predominates and, finally, the catalyst loses most of its activity and isomerization is the only reaction observed. The product distribution obtained suggests that, instead of authentic alkylation, the initial prevalent mechanism is polymerization followed by β-scission.

The adsorption microcalorimetry and FTIR spectroscopy of adsorbed pyridine results for fresh samples demonstrated that USY has the strongest acid sites (both Brønsted and Lewis) and the highest concentration of strong sites, followed by REY and then by Beta zeolite. This order is the opposite of the order observed for the alkylation catalytic performance of these zeolites. In particular, it seems that having a high concentration of strong Lewis sites promotes deactivation. Brønsted sites with intermediate acid strength appear to be the appropriate sites for maintaining good alkylation catalytic performance.

Coke formation significantly decreases the acidity and acid strength of the zeolites studied. A fraction of the intermediate strength sites is lost for all deactivated catalysts studied (specially for Beta), but some strong sites are still available for deactivated USY and

Beta. This evidence supports a contribution of pore blocking or pore filling (deactivation model II) to the deactivation of these zeolites. The deposits formed have a strong paraffinic character, but evidence for olefinic species is also observed. The degree of unsaturation of the surface species formed increases from Beta to USY zeolite implying that the presence of a high concentration of strong Lewis acid sites promotes the formation of unsaturated compounds.

All of these results lead us to propose two deactivation models to explain the deactivation: the direct obstruction of the alkylation active sites by irreversible adsorption of coke precursors; and the indirect obstruction of the active sites by pore blocking or pore filling. Evidence that both processes might be occurring for the catalysts used was obtained from the product distribution as the catalysts deactivate. FTIR spectroscopy results, and from the adsorption microcalorimetry results.

Acknowledgements

We wish to acknowledge the support of a National Science Foundation-RIMI Grant (G.N. HRD-9106637) that allowed us to purchase the microcalorimeter used in this work. In addition, we thank the support of a Department of Energy-EPSCoR Program Grant (G.N. DE-FG02-94ER75764) that allowed us to purchase the FTIR spectrometry used in this work and for partial financial support of one of us (Leda Pernett-Bolaño). Furthermore, we wish to thank the University of Puerto Rico – Mayagües Campus (UPR-RUM) for financial support. We also acknowledge the technical support provided by the UPR-RUM Chemical Engineering and Chemistry Departments. Finally, we appreciate the help provided by W.R. Grace & Co.-Davison Division and Mr. Wilson Suarez for providing zeolite samples and Mobil Research and Development Corp. for donating the syringe pump and a GC used in the initial stages of this work.

References

[1] EPA, Clean Air Act Amendments of 1990. Detailed Summary of Titles, 1990.
[2] J. Weitkamp, in: G. Ohlmann, et al. (Eds.), Catalysis and Adsorption by Zeolites, 21, Elsevier, Amsterdam, 1991.
[3] R.J. Schmidt, P.L. Bogdan, N.L. Gilsdorf, Chemtech Feb. (1993) 41.
[4] I.E. Maxwell, J.E. Naber, Catal. Lett. 32 (1992).
[5] H. Pines, Chemtech, March (1982) 150.
[6] L.F. Albright, Oil & Gas J. 88 (1990) 72.
[7] G. Hoffman, Hydrocarbon Processing, February (1991) 37.
[8] G. Parkinson, Chem. Eng. May (1990) 41.
[9] W.E. Garwook, P.B. Venuto, J. Catal. 11 (1968) 175.
[10] F.W. Kirsch, J.D. Potts, D.S. Barmby, Oil & Gas J. 66 (1968) 120.
[11] F.W. Kirsch, J.D. Potts, Div. Petr. Chem., Amer. Chem. Soc. 15 (No.3, 1970) A109, preprints.
[12] F.W. Kirsch, Lauer J.L. Potts J.D. Div. Petr. Chem., Amer. Chem. Soc. 16 (No. 2 1917) B24, preprints.
[13] F.W. Kirsch, J.D. Potts, D.S. Barmby, J. Catal. 27 (1972) 142.
[14] R. Schöllner, H. Hölzel, J. für Praktische Chemie 317 (1975) 694.
[15] R. Schöllner, H. Hölzel, Zeitschrift Chemie 15 (1975) 469.
[16] Kh. M. Minachev, E.S. Mortikov, S.M. Zenkovsky, N.V. Mostovoy, N.F. Kononov, in: L.F. Albright et al. (Eds.), Industrial and Laboratory Alkylation, ACS Symposium Series, 1977.
[17] G. Gárdos, L. Péchy, Á. Rédey, C. Okonji, Hung. J. Ind. Chem. 8 (1980) 363.
[18] G. Gárdos, L. Péchy, Á. Rédey, I. Sokorai, Hung. J. Ind. Chem. 8 (1980) 371.
[19] J. Weitkamp, in: B. Imelik et al. (Eds.), Catalysis by Zeolites, 65, Elsevier, Amsterdam, 1980.
[20] J. Weitkamp, S. Mixner, Petrochem. Brennst-Chem. 36 (1983) 527.
[21] J. Weitkamp, Acta Chim. Phys. 31 (1985) 271.
[22] H. Pines, in: The Chemistry of Catalytic Hydrocarbon Conversions, Academic Press, New York, 1981.
[23] M. Daage, F. Fajula, Bull. Soc. Chim. Fr. 5 (1984) 153.
[24] Y.F. Chu, A.W. Chester, Zeolites 6 (1986) 195.
[25] A. Corma, A. Martínez, Cat. Rev. Sci. Eng. 35 (1993) 483.
[26] A. Corma, A. Martínez, C. Martínez, J. Catal. 146 (1994) 185.
[27] A. Corma, V. Gómez, A. Martínez, Appl. Catal. A: Gernal 119 (1994) 83.
[28] M. Stöcker, H. Mostad, T. Rørvik, Catal. Lett. 28 (1994) 203.
[29] C. Flego, I. Kiricsi, W.O. Parker Jr., M.G. Clerici, Appl. Catal. A: General 124 (1995) 107.
[30] B. Juguin, F. Raatz, Marcilly, French Patent 2,631,956, 1988.
[31] R.L. Martin, Anal. Chem. 32 (1960) 336.
[32] F.A. Diaz Mondoza, M.S. Thesis, University of Puerto Rico-Mayagüez, 1995.
[33] N. Cardona-Martínez, J.A. Dumesic, J. Catal. 125 (1990) 427.
[34] G. Connell, Ph.D. thesis, University of Wisconsin-Madison, 1985.
[35] P. Pichat, M.-V. Mathieu, B. Imelik, Bull. Soc. Chim. Fr. 8 (1969) 2611.
[36] C.H. Kline, J. Turkevich, J. Chem. Phys. 12 (1944) 300.
[37] D.T. Chen, S.B. Sharma, I. Filiminov, J.A. Dumesic, Catal. Lett. 12 (1992) 201.

[38] N. Cardona-Martínez, J.A. Dumesic, Adv. Catal. 38 (1992) 149.
[39] R. Kumar, W.-C. Cheng, K. Rajagopalan, A.W. Peters, P. Basu, J. Catal. 143 (1993).
[40] G. Alvarez, M.S. Thesis, University of Puerto Rico-Mayagüez, 1993.
[41] K. Tsutsumi, H. Koh, S. Hagiwara, H. Takahashi, Bull. Chem. Soc. Jpn. 48 (1975) 3576.
[42] T. Masuda, H. Taniguchi, K. Tsutsumi, H. Takahashi, Bull Chem. Soc. Jpn. 52 (1979) 2849.
[43] N. Cardona-Martínez, J.A. Dumesic, J. Catal. 128 (1991) 23.
[44] P.C. Gravelle, Thermochim. Acta 96 (1985) 365.
[45] P. Dejaifve, A. Auroux, P.C. Gravelle, J.C. Védrine, Z. Gabelica, E.G. Derouane, J. Catal. 70 (1981) 123.
[46] H.G. Karge, Stud. Surf. Sci. Catal. 58 (1991) 531.
[47] D. Eisenbach, E. Gallei, J. Catal. 56 (1979) 377.